applied sciences

MDPI

Article

Seismic Ground Response Estimation Based on Convolutional Neural Networks (CNN)

Seokgyeong Hong [1], Huyen-Tram Nguyen [1], Jongwon Jung [2] and Jaehun Ahn [1,*]

1 Department of Civil and Environmental Engineering, Pusan National University, Busan 46241, Korea; topkid4140@pusan.ac.kr (S.H.); nhtram153@pusan.ac.kr (H.-T.N.)
2 School of Civil Engineering, Chungbuk National University, Cheongju-si 28644, Korea; jjung@cbnu.ac.kr
* Correspondence: jahn@pusan.ac.kr; Tel.: +82-51-510-7627

Abstract: One of the purposes of earthquake engineering is to mitigate the damages in buildings and infrastructures and, therefore, reduce the impact of earthquakes on society. Seismic ground response analysis refers to the process of evaluating the ground surface motions based on the bedrock motion. On the other hand, deep learning techniques have been developing fast, and they are establishing their application in the civil engineering field. This study proposes two convolutional neural network (CNN) models to estimate the seismic response of the surface based on the seismic motion measured at 100 m level beneath the surface, and selected the one which outperforms the other as the main model. The performances of the main model are compared with those of a physical software SHAKE2000. Twelve sites that include 100 earthquake datasets, whose moment magnitude is higher than 6 and PGA is higher than 0.1 g, were selected. In addition, the corresponding earthquake datasets are used for the CNN model. Whereas the conventional software overestimated the values of the amplitudes for most of the sites, the proposed CNN model predicts fairly well both the values of the amplitudes and the natural periods where responses amplify the most with few exceptions. The proposed model especially outperforms the conventional software when the natural periods range from 0.01 to 0.3 s. For specific sites, the average mean squared errors of the proposed model are even dozens of times lower than those of the conventional physical software.

Keywords: earthquake; seismic ground response analysis; convolutional neural networks; physical analysis software; acceleration response spectrum

Citation: Hong, S.; Nguyen, H.-T.; Jung, J.; Ahn, J. Seismic Ground Response Estimation Based on Convolutional Neural Networks (CNN). *Appl. Sci.* **2021**, *11*, 10760. https://doi.org/10.3390/app112210760

Academic Editor: Amadeo Benavent-Climent

Received: 30 September 2021
Accepted: 3 November 2021
Published: 15 November 2021

1. Introduction

One of the main purposes of modern earthquake engineering is to mitigate damage in buildings and infrastructure and, therefore, reduce the impact of earthquakes on society [1]. When an earthquake occurs at fault, the earthquake waves propagate from the source to other sites. The seismic waves travel through rocks over most of their trip from the source to the ground surface, and they finally reach the surface through the soil. As the soil deposits tend to act as filters to seismic waves by amplifying motion at certain frequencies and attenuating it at others, characteristics of the soil mainly influence the nature of shaking at the ground surface, which is called the site effect [2,3]. Evaluating the local site effect on ground shaking is an essential part of earthquake-resistant design [4]. Seismic ground response analysis refers to the process of evaluating the ground surface motions based on the bedrock motion to consider the local site effect [5]. One-dimensional seismic ground response analyses with wave equations have been widely performed in practices [6].

Since Adeli and Yeh (1989) published the first article on applications of neural networks to structural design [7], a large number of research have been conducted on civil engineering applications of neural networks. In particular, convolutional neural networks (CNN), a class of artificial neural networks commonly applied to analyze visual imagery, can extract features from raw data [8]. Perol et al. (2018) detected earthquake occurrences and locations of epicenters in a predefined area with seismic waveforms recorded on a seismic station using CNN [9]. Ross et al. (2018) trained the CNN model on the vast data archives of the Southern California Seismic Network to detect seismic body-wave phases [10]. Mousavi et al. (2019) introduced the CNN-Recurrent neural networks Earthquake detector (CRED), a combination of convolutional layers and bi-directional long-short-term memory units in a residual structure [11]. Wu and Jahanshahi (2019) proposed a CNN-based approach to evaluate the dynamic response of a linear single-degree-of-freedom (SDOF) system, a nonlinear SDOF system, and a full-scale, three-story, multi-degree-of-freedom (MDOF) steel frame [12]. Harirchian et al. (2021) presented a review on the application of soft computing techniques for the rapid visual safety evaluation and damage classification of an existing building [13]. Li et al. (2021) utilized CNN to tune the first approximation to predict the maximum interstory drift ratio (MIDR) [14].

Although research on the application of artificial neural networks to structural design has been actively conducted, the application to the seismic ground response analysis is insufficient. This study suggests two convolutional neural networks (CNN) models, which estimate the seismic response of the surface based on the seismic motion measured at the bed rock in a site, and selects the one which outperforms the other as the main model. The performances of the main model in each site are compared with those of conventional analysis software for every selected site.

2. Earthquake Database

Since the National Research Institute for Earth Science and Disaster Prevention (NIED) in Japan has applied seismometers on boreholes and surfaces in each station to record earthquakes throughout the nation, the strong-motion seismograph network Kiban Kyoshin Network (KiK-net) presents the acceleration history measurements, information of the sites, and earthquake events required to perform the seismic ground response analysis [15–17].

2.1. Site Information

A total of 12 sites that include 50 earthquake events, whose magnitude is higher than 6 and PGA is greater than 0.01 g, were selected (Figure 1). These sites have the records at both surfaces and at 100 m depth beneath the surface after the year 2008.

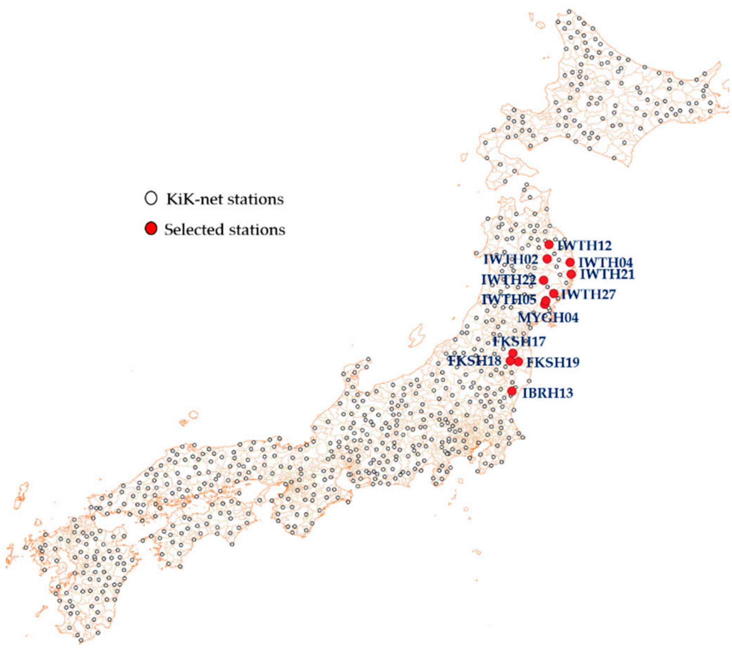

Figure 1. The selected stations.

Shear wave velocity (V_S) profiles and brief classifications of the soil layers of the selected sites were shown in Figure 2. The black triangles in the figure represent the installation locations of the seismometers.

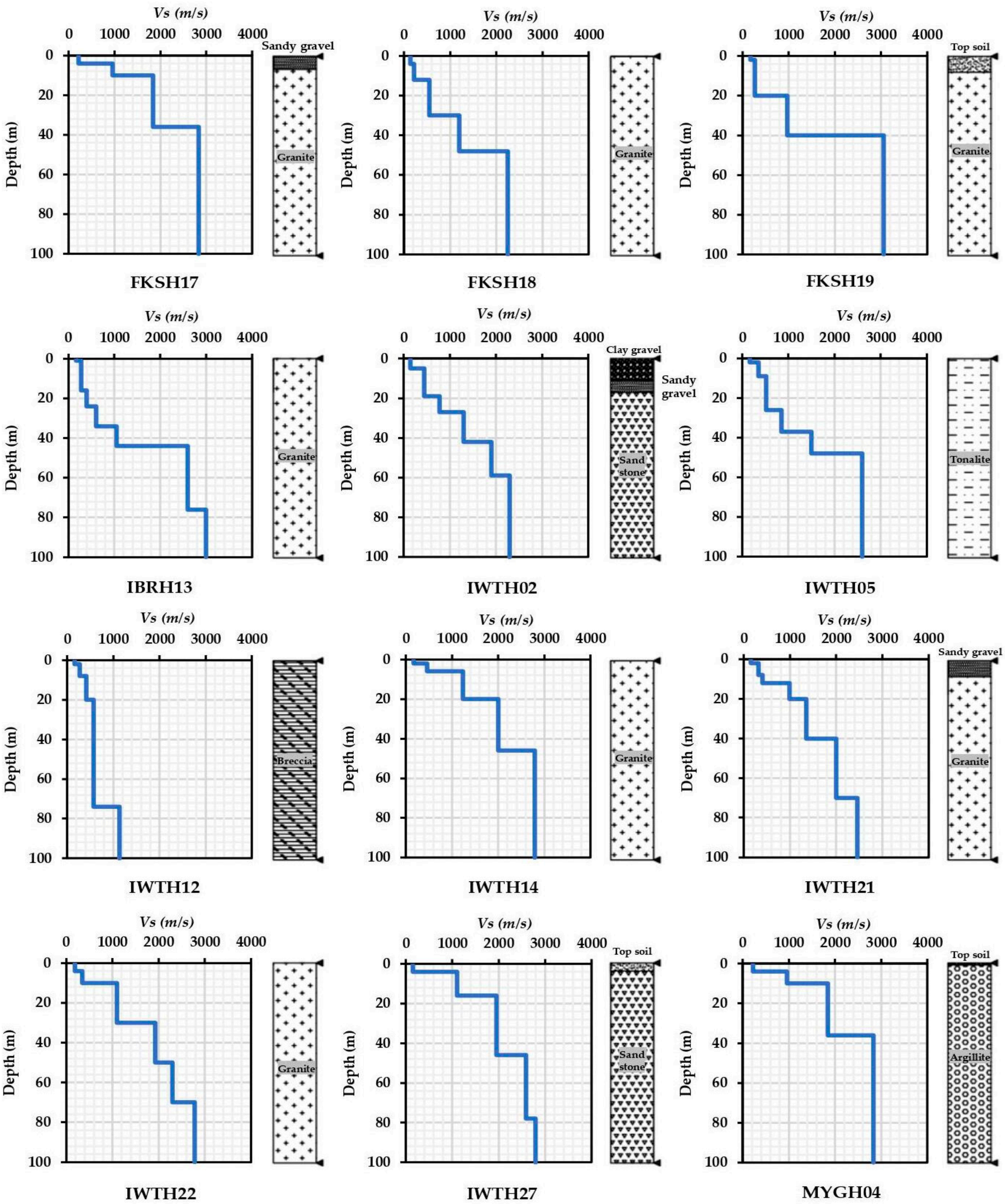

Figure 2. Soil profiles and shear wave velocities at the selected sites.

According to a two-parameter site classification system from the National Earthquake Hazard Reduction Program (NEHRP), the sites can be classified into six classes based on the average shear velocity ($V_{S,30}$) and natural period of the soil deposit (T_G) [18] in the seismic design. The average shear velocity is the shear wave velocity profile up to 30 m (100 ft) depth beneath the ground. The average shear velocity and the natural period of the soil can respectively be calculated by Equations (1) and (2):

$$V_{S,30} = \frac{30}{\sum_{i=1}^{n} \frac{D_i}{V_{Si}}} \tag{1}$$

$$T_G = 4\sum_{i}^{n} \frac{D_i}{V_{Si}} \tag{2}$$

where n is the number of strata from the surface up to 30 m beneath the ground surface, D_i is the thickness of the ith stratum (m), and V_{Si} is the shear wave velocity of the ith stratum (m/s).

According to the National Earthquake Hazard Reduction Program (NEHRP), the sites where $V_{S,30}$ ranges from 180 to 360 m/s are classified as stiff soil. The sites where $V_{S,30}$ ranges from 360 to 760 m/s are classified as soft rock, and those whose $V_{S,30}$ are over 760 m/s are classified as rock. Table 1 presents the basic information of the sites, the values of average shear velocities, natural periods, and the classification of the soil in the sites.

Table 1. Information of the sites.

No.	Site Code	Site Name	$V_{S,30}$ (m/s)	NEHRP Site Classification	Description	T_G (s)
1	FKSH17	Kawamata	544.0	C	Dense soil, Soft rock	0.22
2	FKSH18	Miharu	307.2	D	Stiff soil	0.39
3	FKSH19	Miyakoji	338.1	D	Stiff soil	0.35
4	IBRH13	Takahagi	335.4	D	Stiff soil	0.36
5	IWTH02	Tamayama	816.3	B	Rock	0.15
6	IWTH05	Fujisawa	442.1	C	Dense soil, Soft rock	0.27
7	IWTH12	Kunohe	367.9	C	Dense soil, Soft rock	0.33
8	IWTH14	Taro	816.3	B	Rock	0.15
9	IWTH21	Yamada	521.1	C	Dense soil, Soft rock	0.23
10	IWTH22	Towa	532.1	C	Dense soil, Soft rock	0.23
11	IWTH27	Rikuzentakata	670.3	C	Dense soil, Soft rock	0.18
12	MYGH04	Towa	849.8	B	Rock	0.14

2.2. Earthquake Events

Fifty earthquake events, whose moment magnitude is higher than 6 and PGA is greater than 0.01 g recorded after the year 2008 in each site, were adopted. As each earthquake was measured in both east-west and north-south directions, they provided 100 datasets of ground motion acceleration histories. A dataset consists of the acceleration history measured at 100 m beneath the surface (bedrock) and the history measured on the ground surface. For the motions at the bedrock, the velocity and displacement histories were generated from the acceleration histories, and they were all assigned to the input data. For the motions on the surface, the acceleration histories were assigned to the output data. Correction of earthquake data was processed with a methodology with a polynomial linear baseline correction and bandpass filter proposed by BAP (Converse, 1982) [19] (Figure 3).

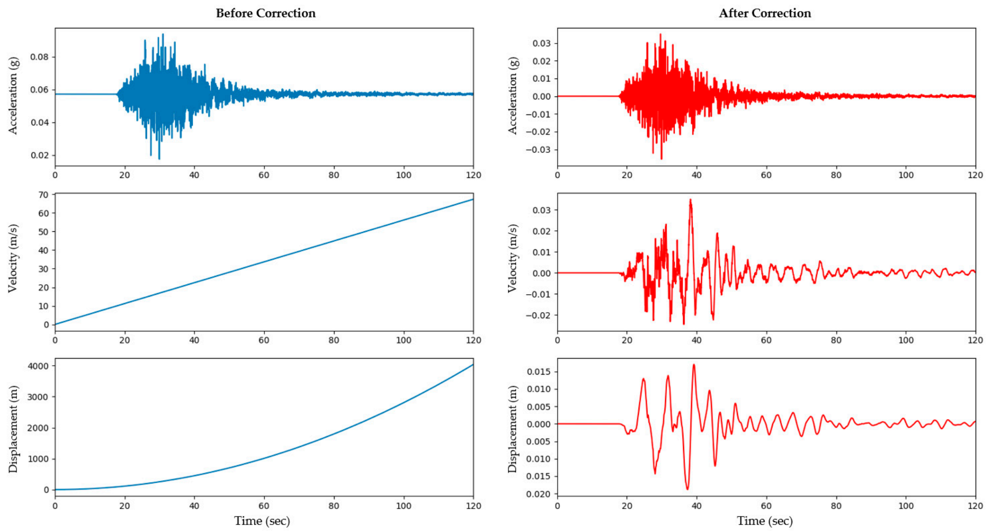

Figure 3. Earthquake data before and after correction (MYGH04).

3. Analytical Method

The study aims at proposing convolutional neural networks (CNN) models to estimate the seismic response of the surface based on the seismic motion measured at bedrock. The software, SHAKE2000, is utilized to compare the performance of proposed models with its performance.

3.1. Seismic Ground Response Analysis

Seismic ground response analysis is used to predict the seismic behavior on the ground surface influenced by the properties of soil deposits [3]. The one-dimensional ground response analysis, which is a simulation of shear waves propagating vertically through shallow soil layers on the assumption that all boundaries are horizontal, is an approach to capture site effects on ground shaking [3,4]. A series of one-dimensional ground response analyses (linear and equivalent linear methods) are introduced.

In the linear method, the material properties are assumed to remain constant during shaking [20]. The material properties are assumed to be unchanged in dynamic processes during the earthquake. The equivalent linear method, initially proposed by Seed and Idriss (1970), accounts for material yielding and damping by iteratively matching the shear modulus and damping ratio to a characteristic strain level [20]. Both are in the frequency domain with linear visco-elastic material behavior. A ground motion time history of the bedrock (input) is converted to the frequency domain by the fast Fourier transform (FFT) algorithm and then multiplied by the transfer function to generate the ground surface motion (output) Fourier series. Thereafter, the ground surface (output) can be transformed back into the time domain by the inverse fast Fourier transform (IFFT), as shown in Equation (3):

$$a_{output}(t) = IFFT\left[f(w) * FFT\left[a_{input}(t)\right]\right] \tag{3}$$

$$f(w) = \frac{u_{output}(\omega)}{u_{input}(\omega)} \tag{4}$$

where $a_{output}(t)$ is ground surface acceleration, $a_{input}(t)$ is bedrock acceleration, and $f(w)$ is a bedrock-to-surface transfer function, as shown in Equation (4). u_{output} is ground surface displacement, and u_{input} is bedrock displacement.

3.2. Convolutional Neural Networks (CNN)

Deep learning explores complex structures in the large dataset using algorithms to change the internal parameters in order to compute the representation of the dataset in each layer from the previous layer, based on the artificial neural networks. Convolutional neural networks (CNN), a class of artificial neural network that has become dominant in computer vision works, are designed to learn spatial hierarchies of features in the form of 2D images automatically and adaptively through backpropagation using building blocks, such as convolution layers, pooling layers, and fully connected layers, as shown in Figure 4 [21]. A convolution layer has image data abstracted to a feature map, and a pooling layer reduce the dimensions of the feature map.

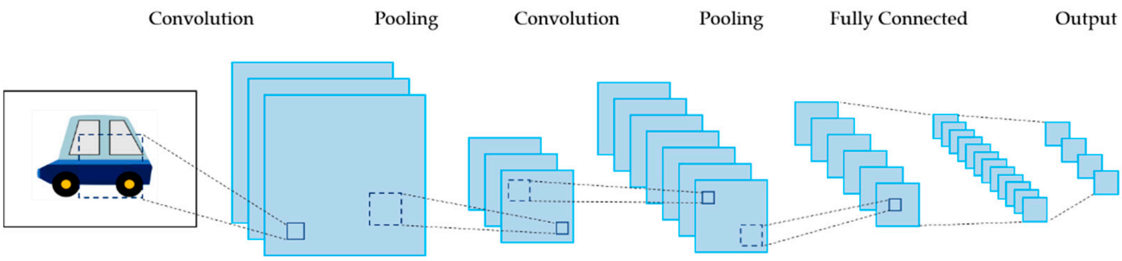

Figure 4. Scheme of the process of convolutional neural networks.

3.3. Response Spectrum

Response spectrum is a plot of the peak response of a series of SDOF systems with varying natural frequencies that provides practical information for the seismic design of structures [22,23]. Based on the response spectrum, ground response measurements and predictions by the analysis program and proposed CNN models are compared.

4. Analytical Procedure

4.1. CNN Model

For the motions measured at the bedrock, velocity histories were calculated by integrating the acceleration histories over time, and displacement histories were calculated by integrating the velocity histories over time. They were assigned to input data, and the acceleration histories measured at the surface were to output data. Every motion applied to the model was tailored to have 12,000 acceleration values measured at time increments of 0.01 s, having 120 s duration. Among the 100 datasets, 80 datasets were used for the train (train dataset), and 20 datasets were for the test (test dataset). Two different CNN models, A and B, were established and tried with the earthquake datasets for site FKSH18. Between them, a model which outperformed the other was selected as a main model.

4.1.1. Model A

Time domain acceleration, velocity, and displacement histories were applied to model A. Every history was evenly split into 120 signals with 100 acceleration values of time increments of 0.01 s, having 1 s of duration. The thin lines behind the graphs in Figure 5 split the signals from the duration of 120 to 1 s. Accordingly, the split time domain acceleration, velocity, and displacement histories at the bedrock are assigned to input data, and the split acceleration histories measured on the surface are to output data, as presented in Figure 5. CNN architecture A consists of a convolution layer with 100 kernels with the size (9,1) as parameters without a pooling layer. Mean squared error (MSE) was adopted to loss function and Rectified linear unit (ReLU) was to activation function.

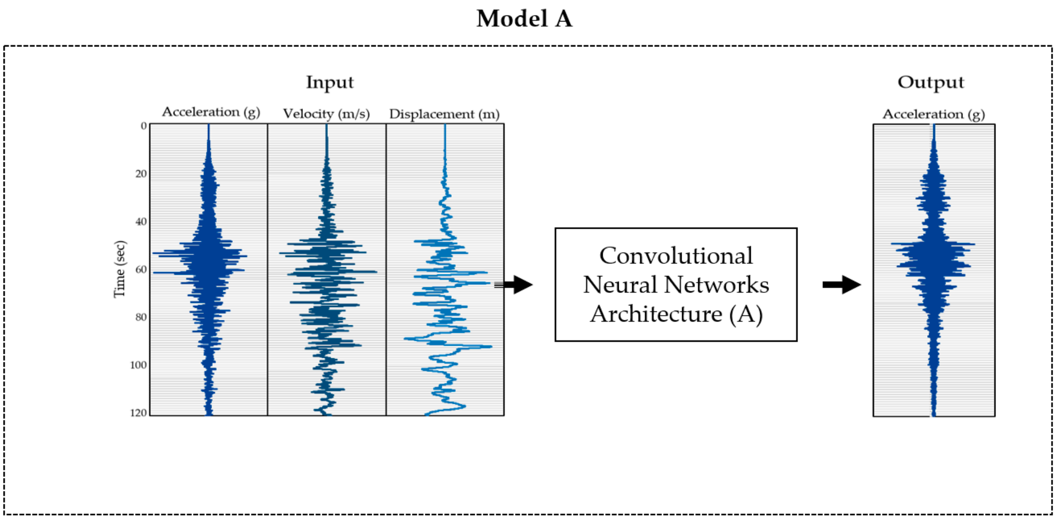

Figure 5. Overview of model A.

4.1.2. Model B

The response spectra of ground motion data were applied to model B. Five percent of damped acceleration, velocity, and displacement response spectra were generated from the time domain acceleration, velocity, and displacement histories at the bedrock, as presented in Figure 6. In addition, they were assigned to input data. Five percent of damped acceleration response spectra calculated from acceleration histories measured on the surface were for output data. The process of model B is shown in Figure 7. CNN architecture B consists of a convolution layer with 500 kernels with the size (21,1) without a pooling layer. Mean squared error (MSE) was also adopted to loss function and Rectified linear unit (ReLU) was to activation function.

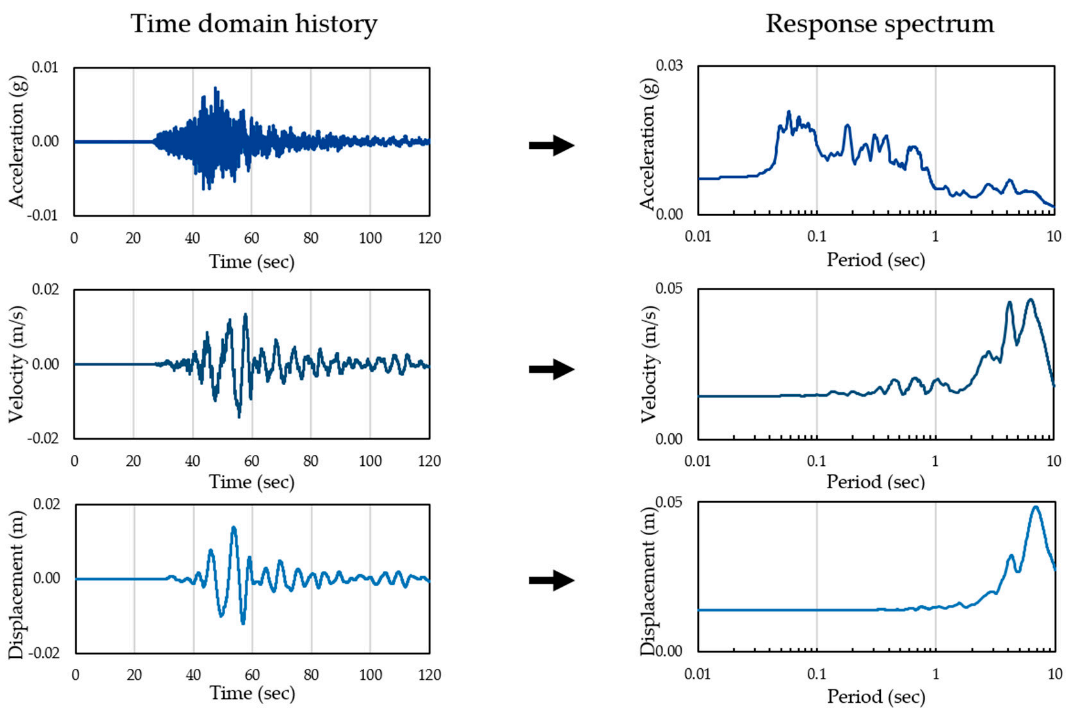

Figure 6. Input data preprocessing for model B.

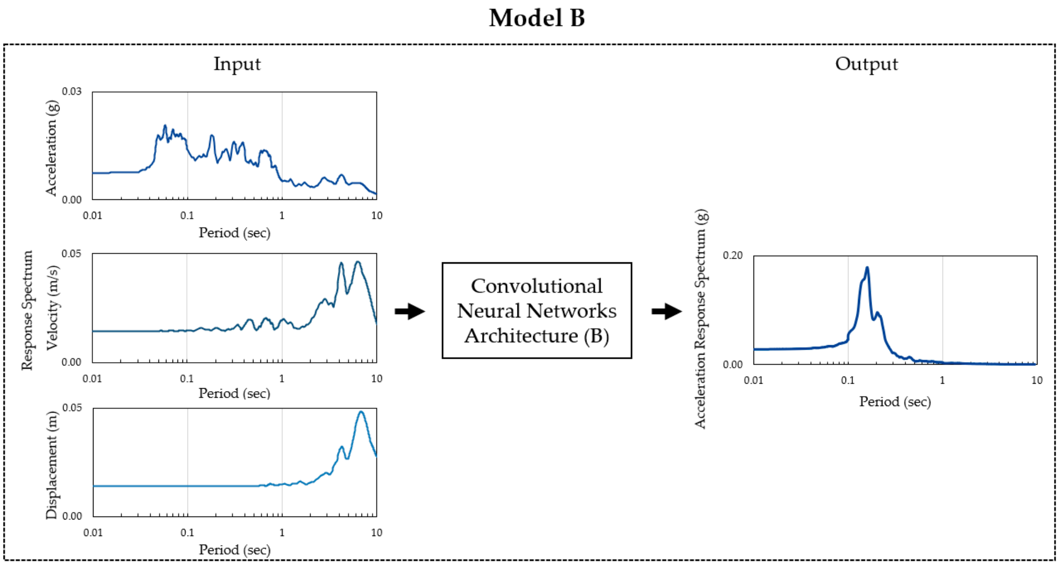

Figure 7. Overview of model B.

After predicting the ground response on the surface through model B, a weight moving average is applied to the prediction for reducing noise and errors. The moving average is used to analyze data points by creating a series of averages of different subsets of the entire dataset. Equation (5) presents the mathematical calculation of the weight moving average we implemented.

$$SA_{pre_i} = \frac{1Sa_{pre_{i-4}} + 2Sa_{pre_{i-3}} + 3Sa_{pre_{i-2}} + 4Sa_{i-1} + 5Sa_{pre_i} + 4Sa_{pre_{i+1}} + 3Sa_{pre_{i+2}} + 2Sa_{pre_{i+3}} + 1Sa_{pre_{i+4}}}{25} \quad (5)$$

where Sa_{pre_i} is the ith prediction of a ground motion by model B, and SA_{pre_i} is the prediction after applying the weight moving average.

4.1.3. Comparisons

With the earthquake dataset in site FKSH 18, CNN models A and B for the site were trained. Each model predicted the ground response at the surface and the results were compared with the baseline to decide main model. Among 20 predictions by each model, the response spectrum of a sample prediction is presented in Figure 8.

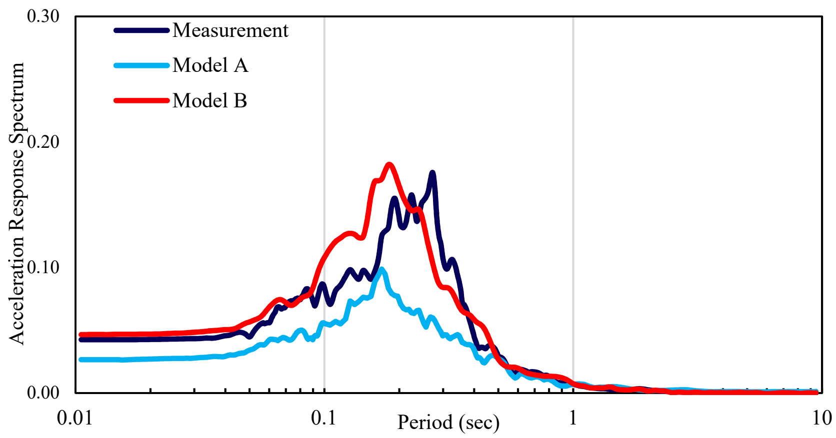

Figure 8. The sample prediction by models A and B and the measurement (FKSH18).

It is found that model B outperforms model A. Not only the average errors of model B were lower than those of model A, but also data processing for model B was more convenient. Whereas the constitution of model A requires the tailored earthquake data with the same duration (120 s) and the same number of values (12,000), model B doesn't. As a result, the study decided to apply model B for the seismic ground response estimation. The study chose model B as a main model, and trained each CNN model for every selected site.

4.2. Conventional Model

The equivalent linear ground response analyses were performed with the analysis program, SHAKE2000, computing the response in a system of homogenous, visco-elastic layers of infinite horizontal extent. The seismic response was calculated by an iterative process in which the shear modulus and damping ratio are updated in each step for the corresponding value of effective shear strain. The effective shear strain was taken as 65% of the maximum shear strain obtained from the calculated strain history. The thin layers are recommended to capture the highly non-uniform variation in strain vs. depth. Therefore, the layers were divided into more than one sublayer, which meets the criteria as Equation (6) [24]:

$$Thickness\ of\ sublayers < \frac{V_S}{4 * f_{max}} \tag{6}$$

where V_S is the shear wave velocity of layers, and f_{max} is maximum frequency.

Widely used soil properties were employed from the previous works of literature. According to the material type of layers, they were classified as rock, gravel, and sand, as shown in Table 2. For the rock, the mean values of normalized shear modulus and damping ratio curves by Schnabel (1973) were taken. For the gravel, the properties by Seed et al. (1986) were taken, and for the sand, those by Seed and Idriss (1970) were taken [25–28]. Figure 9 shows the adopted mean values of normalized shear modulus and damping ratio curves.

Table 2. Classification and reference according to the material type.

Material Type	Classification	Reference
Argillite Breccia Granite Sandstone Tonalite	Rock (Mean)	Schnabel (1973)
Sandy gravel Clayey gravel	Gravel (Mean)	Seed et al. (1986)
Top soil	Sand (Mean)	Seed and Idriss (1970)

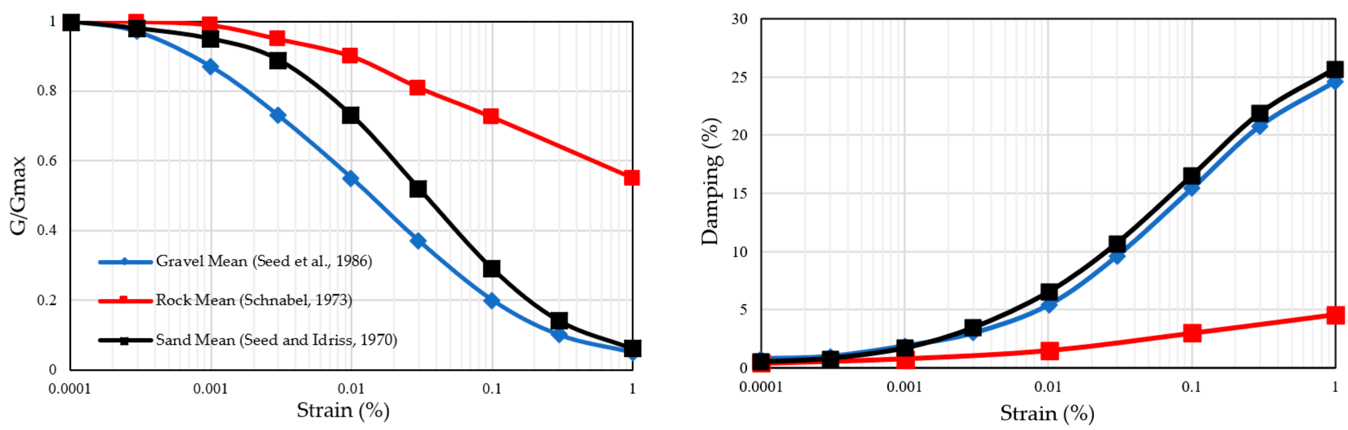

(**a**) (**b**)

Figure 9. Dynamic soil properties: (**a**) Normalized shear modulus reduction curves; (**b**) damping ratio curves.

5. Results

5.1. Prediction

Among the results from 20 testing datasets for each site, response spectra of 6 sample results are presented in Figures 10–21. The name of the subfigure in the figures are the original name from the source of data, KiK-net.

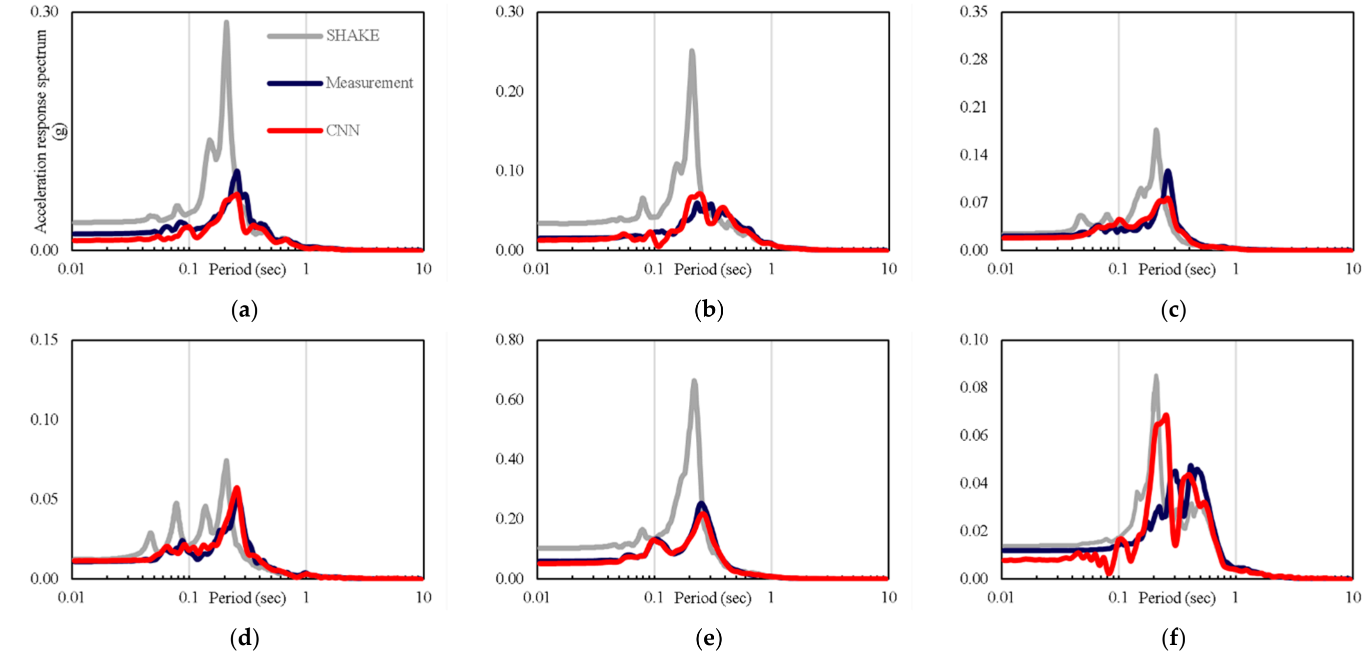

Figure 10. The six samples of acceleration response spectra measurements and predictions at site FKSH17. (**a**) FKSH171201011428.EW. (**b**) FKSH171201011428.NS. (**c**) FKSH171204131910.EW. (**d**) FKSH171206180532.NS. (**e**) FKSH171305181448.EW. (**f**) FKSH171309040919.NS2.

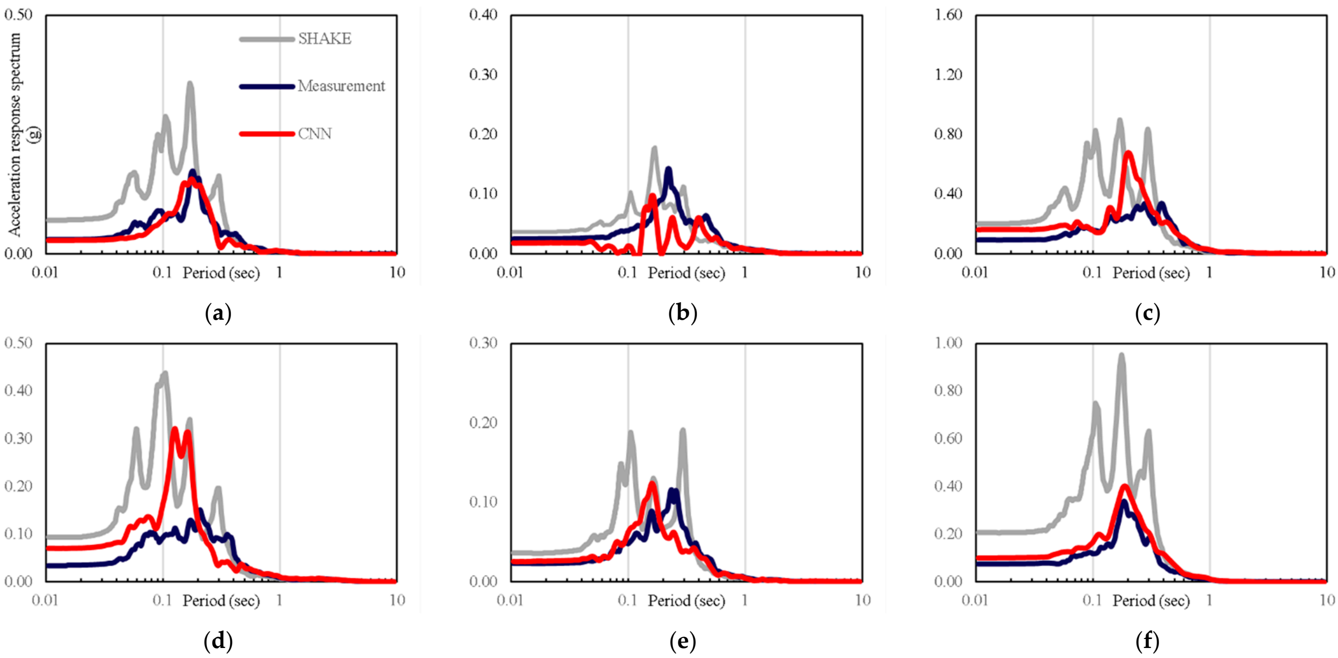

Figure 11. The six samples of acceleration response spectra measurements and predictions at site FKSH18. (**a**) FKSH181310260210.EW. (**b**) FKSH181407120422.NS. (**c**) FKSH181611220559.NS. (**d**) FKSH181612282138.NS. (**e**) FKSH181906182222.NS. (**f**) FKSH181908041923.EW.

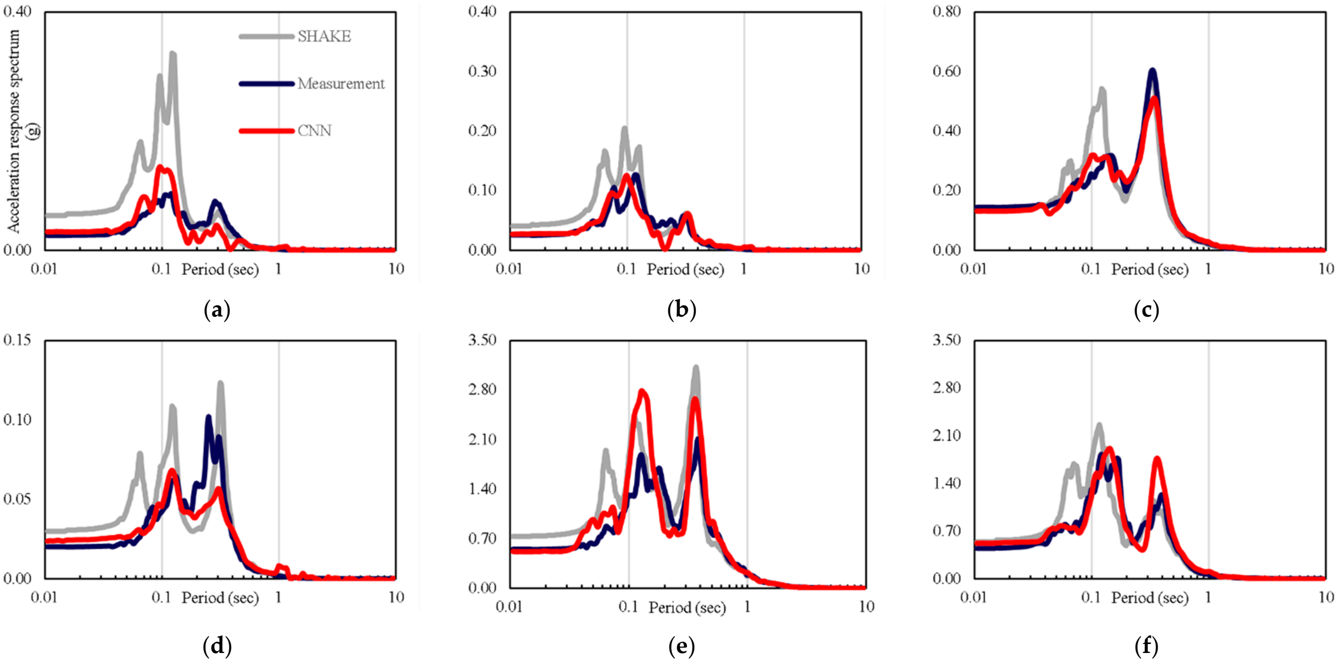

Figure 12. The six samples of acceleration response spectra measurements and predictions at site FKSH19. (**a**) FKSH191611240623.EW. (**b**) FKSH191611240623.NS. (**c**) FKSH191908041923.EW. (**d**) FKSH192004200539.NS. (**e**) FKSH192102132308.EW. (**f**) FKSH192102132308.NS.

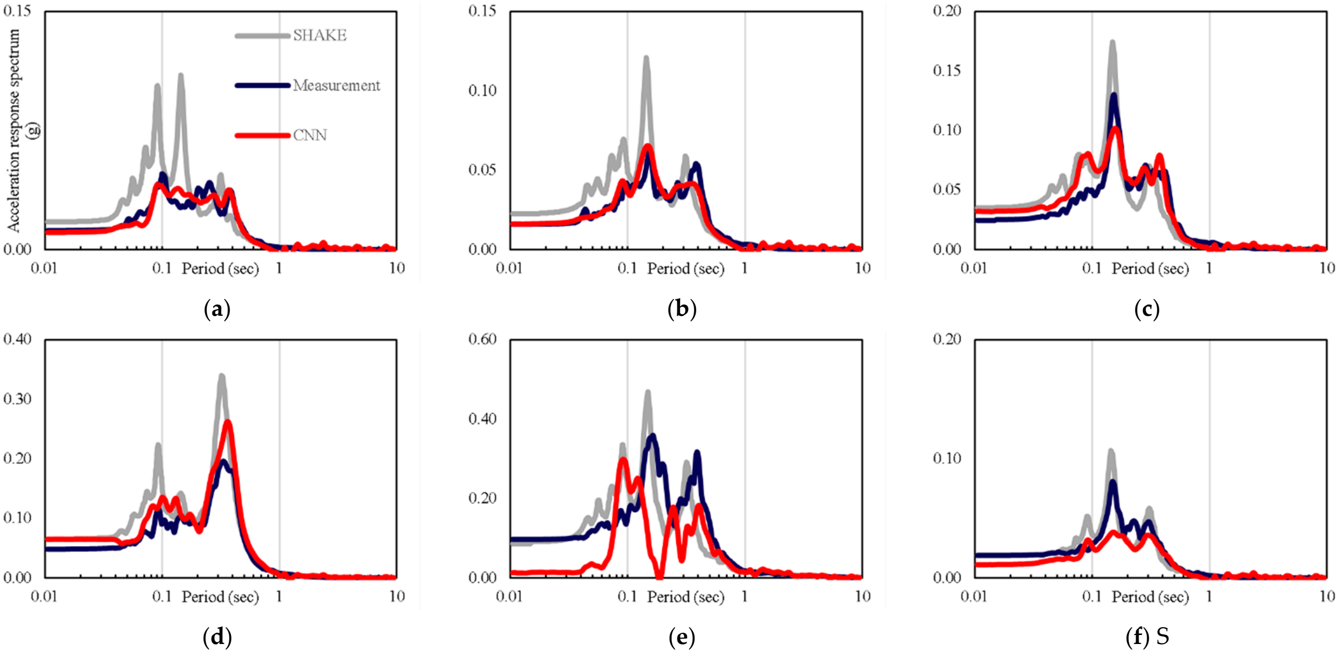

Figure 13. The six samples of acceleration response spectra measurements and predictions at site IBRH13. (**a**) IBRH131412201830.EW. (**b**) IBRH131412201830.NS. (**c**) IBRH131611240623.NS. (**d**) IBRH131908041923.EW. (**e**) IBRH131611220559.NS. (**f**) IBRH132006250447.NS.

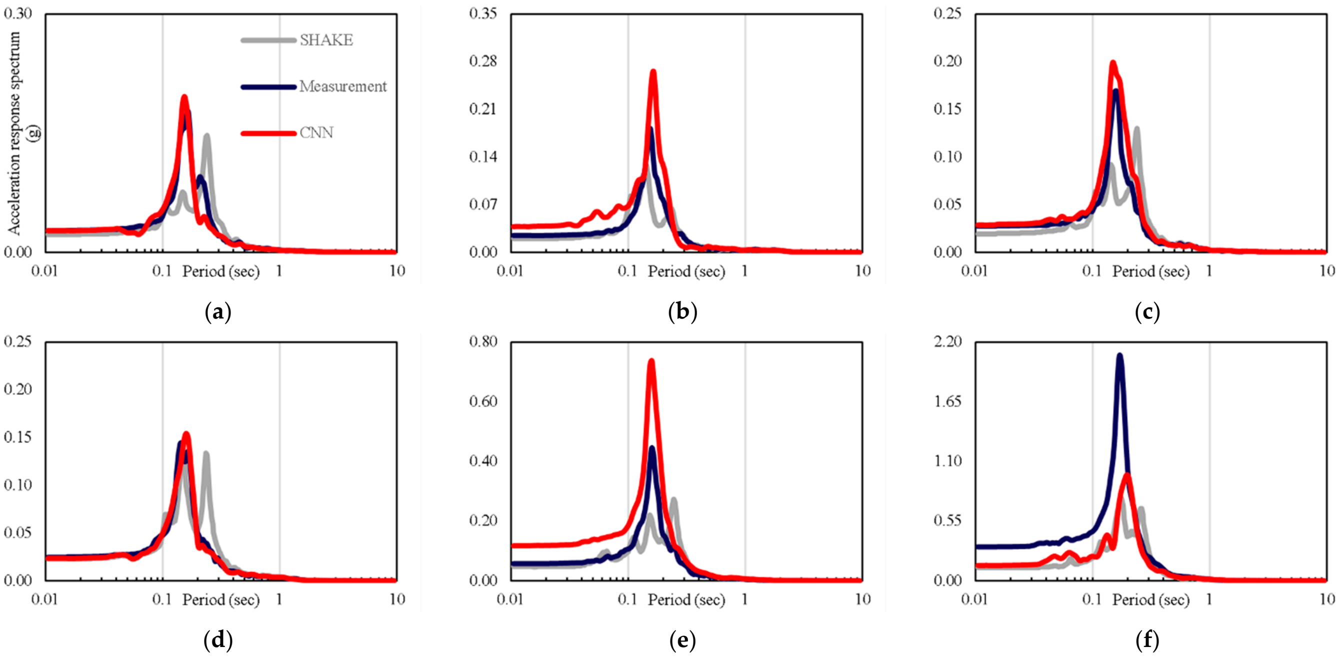

Figure 14. The six samples of acceleration response spectra measurements and predictions at site IWTH02. (**a**) IWTH021809060308.EW. (**b**) IWTH021906182222.EW. (**c**) IWTH021908041923.EW. (**d**) IWTH021908041923.NS. (**e**) IWTH022004200539.EW. (**f**) IWTH022105011027.EW.

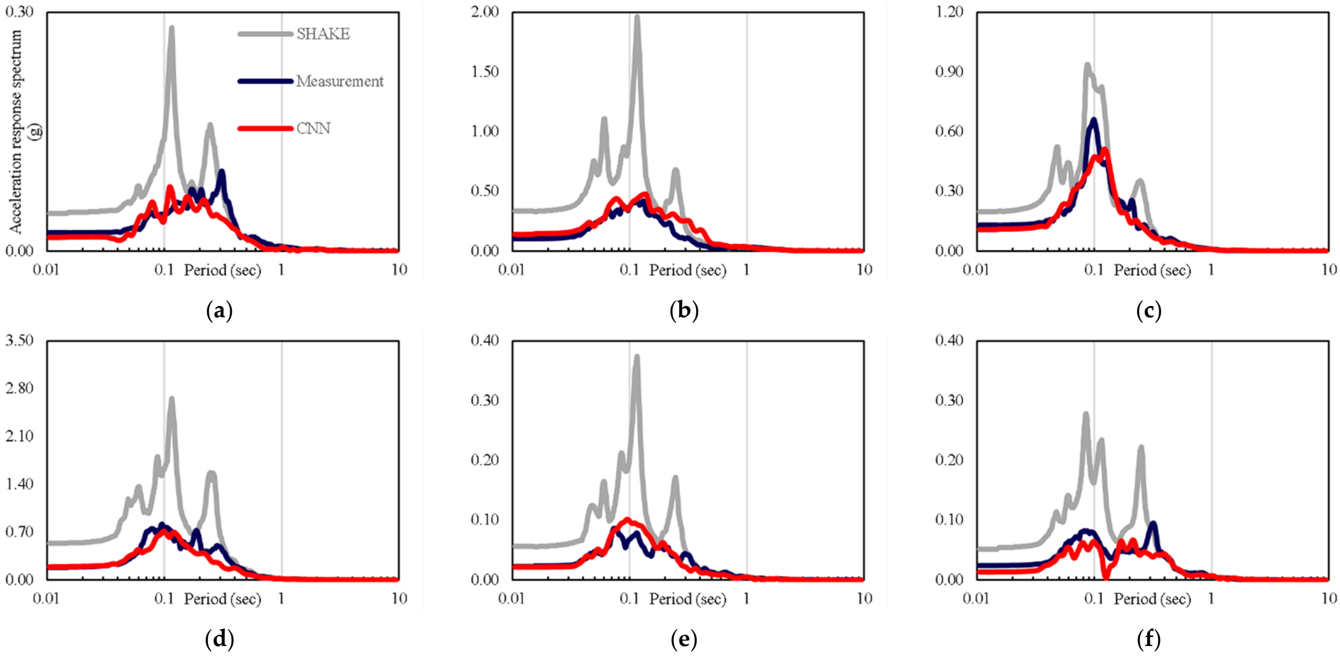

Figure 15. The six samples of acceleration response spectra measurements and predictions at site IWTH05. (**a**) IWTH051502170806.EW. (**b**) IWTH051505130613.EW. (**c**) IWTH052009121144.EW. (**d**) IWTH052102132308.NS. (**e**) IWTH052105140858.EW. (**f**) IWTH052105140858.NS.

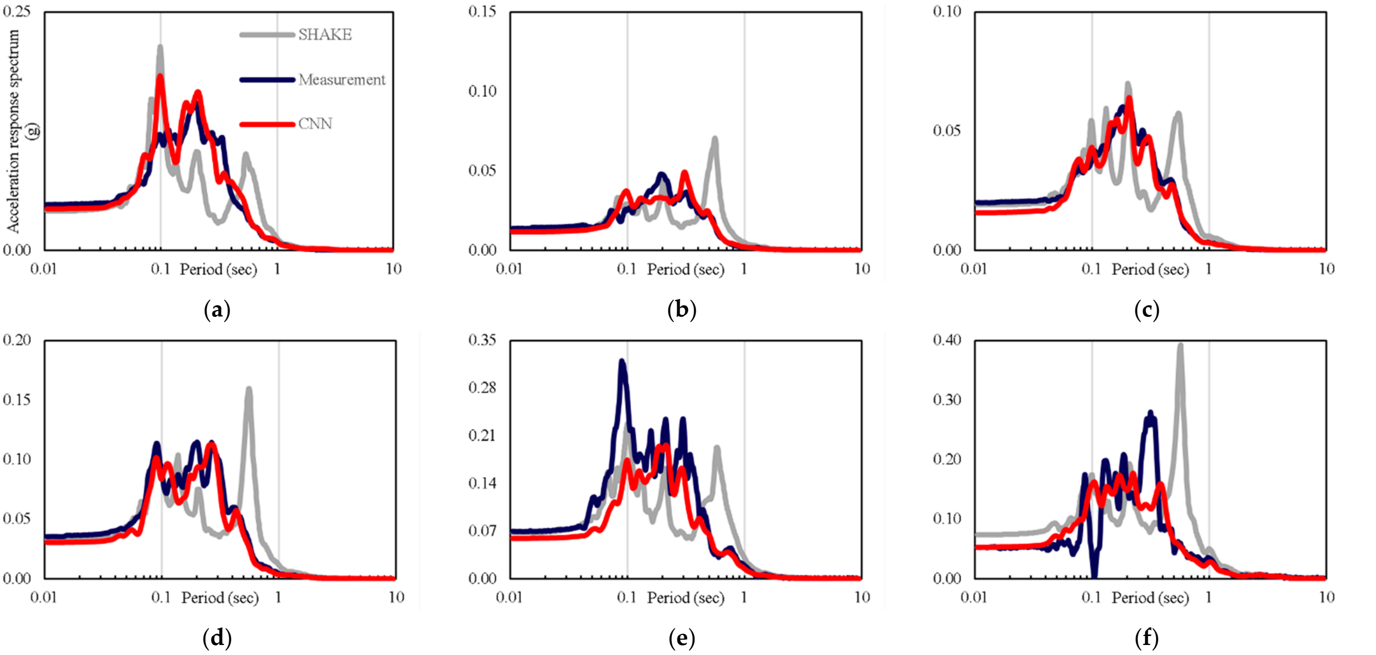

Figure 16. The six samples of acceleration response spectra measurements and predictions at site IWTH12. (**a**) IWTH121801241951.EW. (**b**) IWTH121908290846.NS. (**c**) IWTH122002131934.EW. (**d**) IWTH122004200539.NS. (**e**) IWTH122012210223.EW. (**f**) IWTH122102132308.EW.

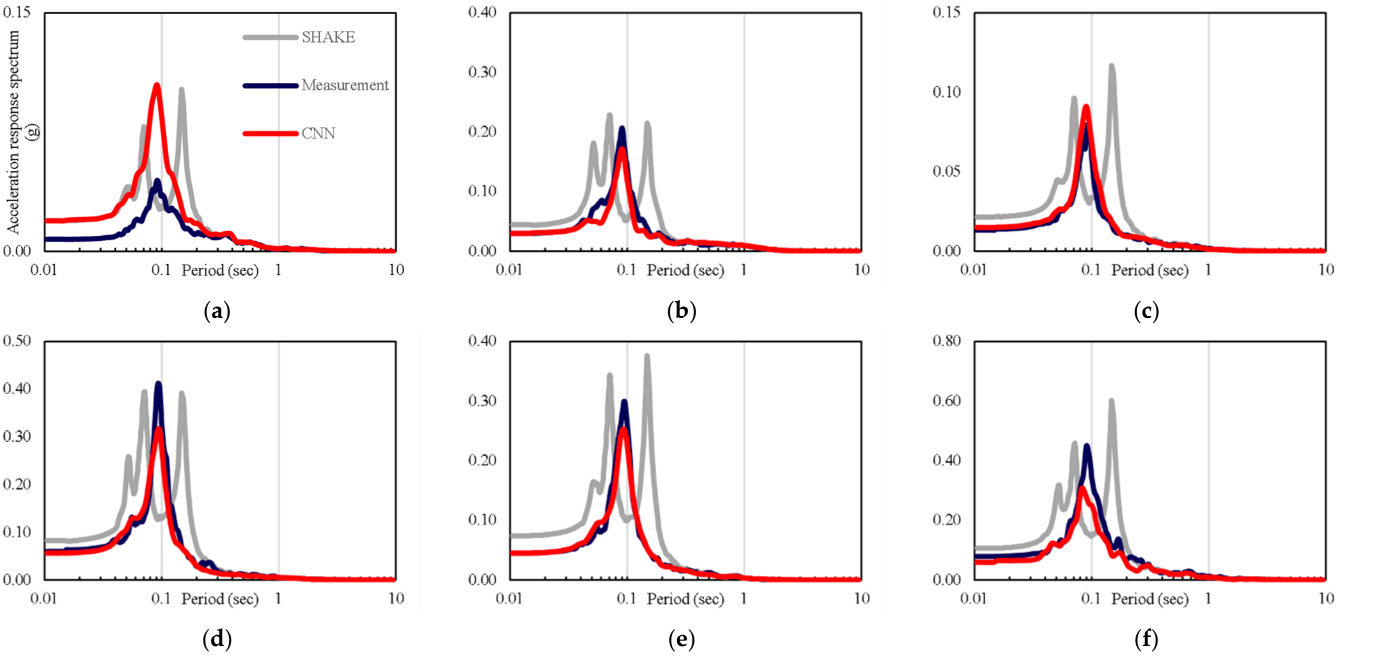

Figure 17. The six samples of acceleration response spectra measurements and predictions at site IWTH14. (**a**) IWTH141601141225.EW. (**b**) IWTH141709270522.NS. (**c**) IWTH141908041923.NS. (**d**) IWTH142004200539.NS. (**e**) IWTH142009121144.NS. (**f**) IWTH142102132308.EW.

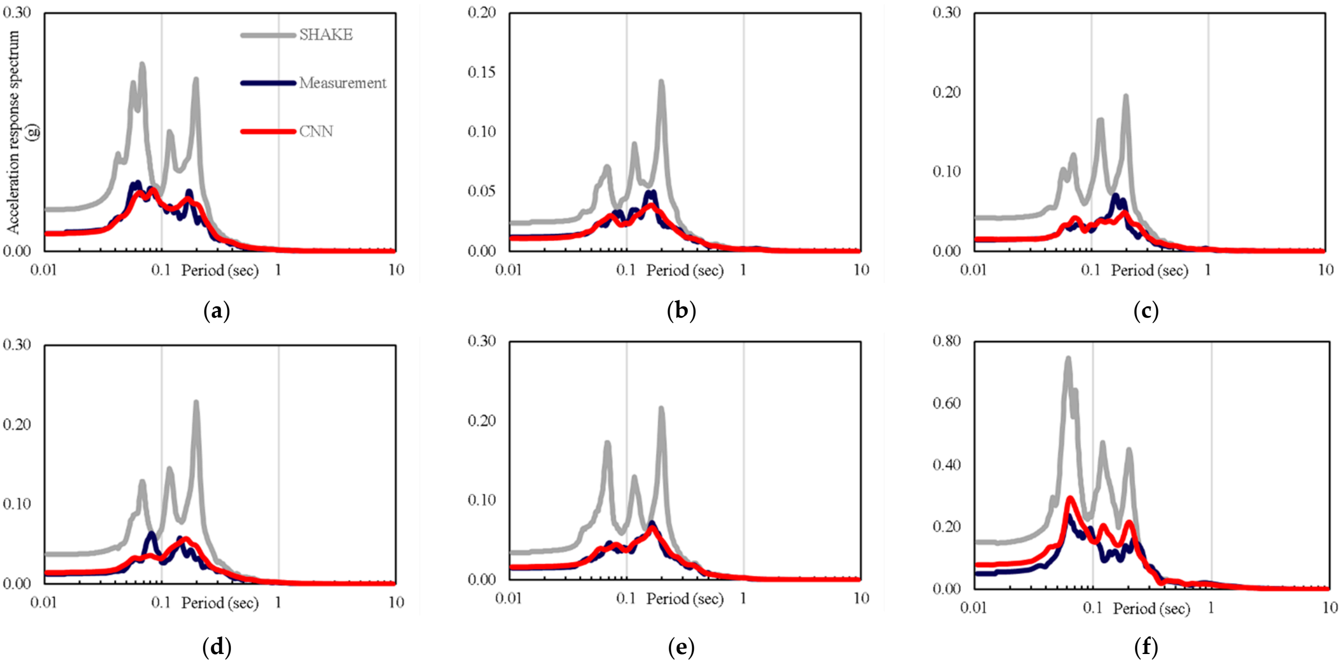

Figure 18. The six samples of acceleration response spectra measurements and predictions at site IWTH21. (**a**) IWTH211310260210.EW. (**b**) IWTH211601141225.EW. (**c**) IWTH211611220559.NS. (**d**) IWTH211801241951.NS. (**e**) IWTH211908041923.NS. (**f**) IWTH212004200539.EW.

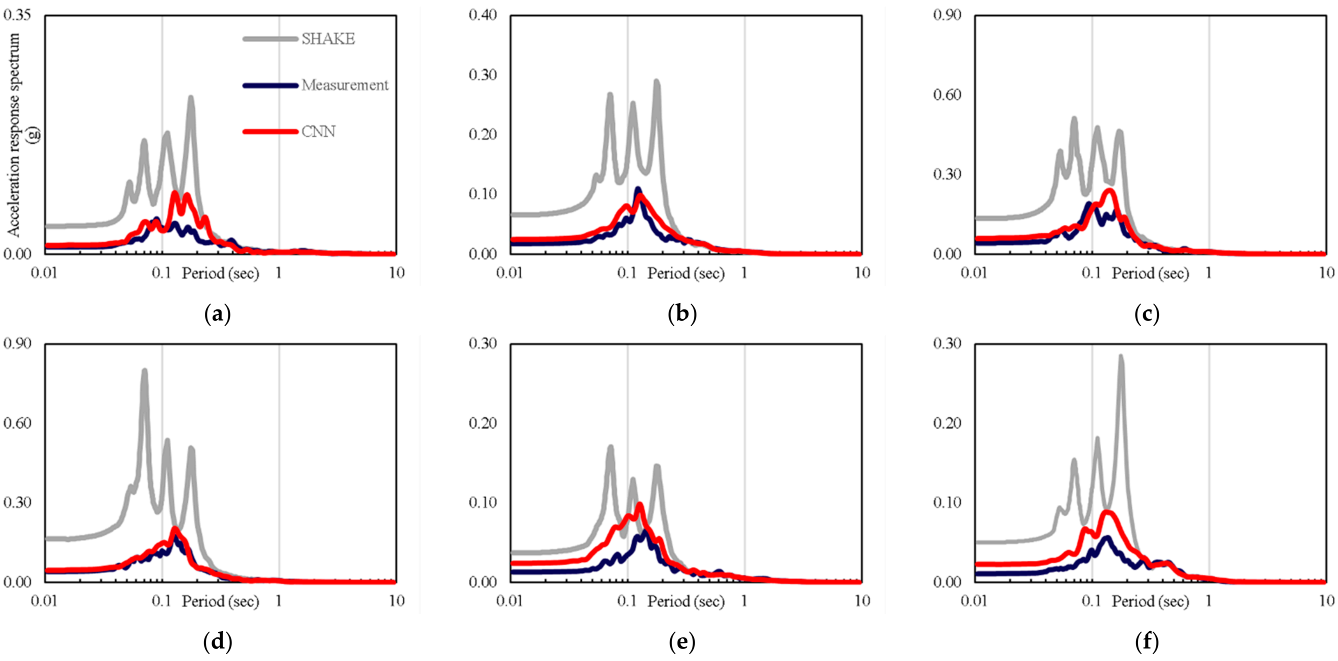

Figure 19. The six samples of acceleration response spectra measurements and predictions at site IWTH22. (**a**) IWTH221611220559.EW. (**b**) IWTH221709270522.NS. (**c**) IWTH222004200539.EW. (**d**) IWTH222004200539.NS. (**e**) IWTH222012210223.NS. (**f**) IWTH222105140858.NS.

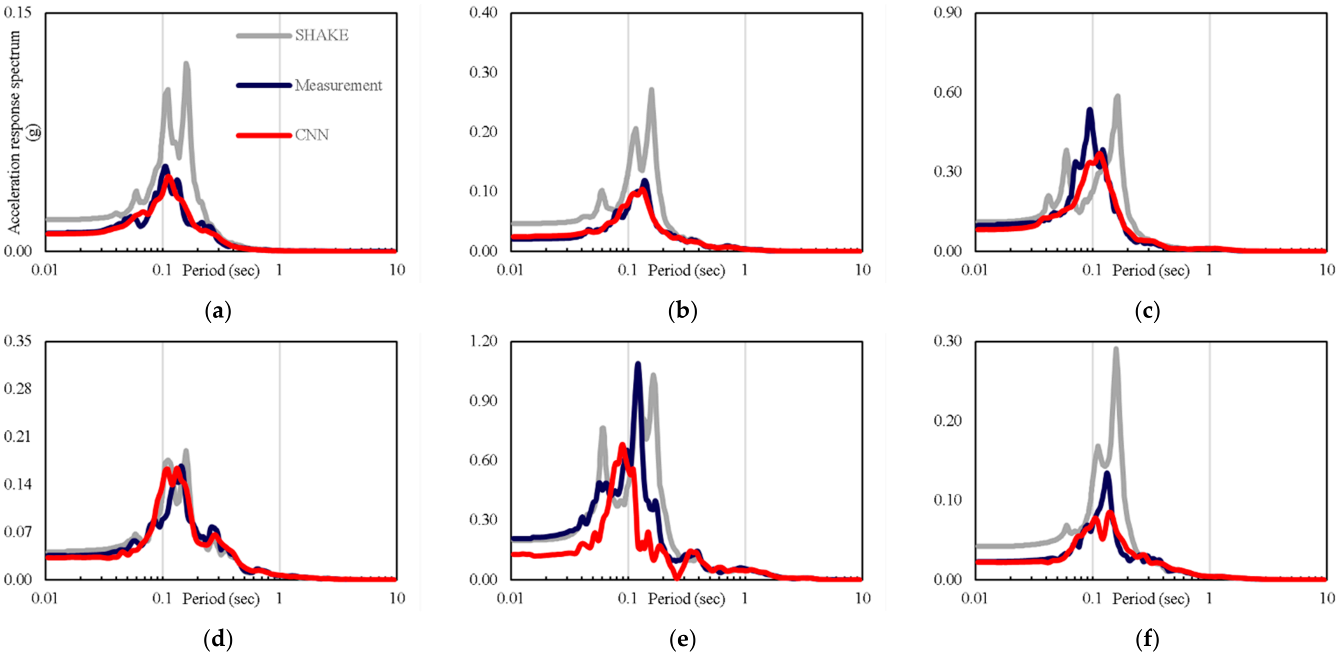

Figure 20. The six samples of acceleration response spectra measurements and predictions at site IWTH27. (**a**) IWTH271212071731.EW. (**b**) IWTH271302022317.EW. (**c**) IWTH271308041229.NS. (**d**) IWTH271502170806.EW. (**e**) IWTH271505130613.EW. (**f**) IWTH271709270522.EW.

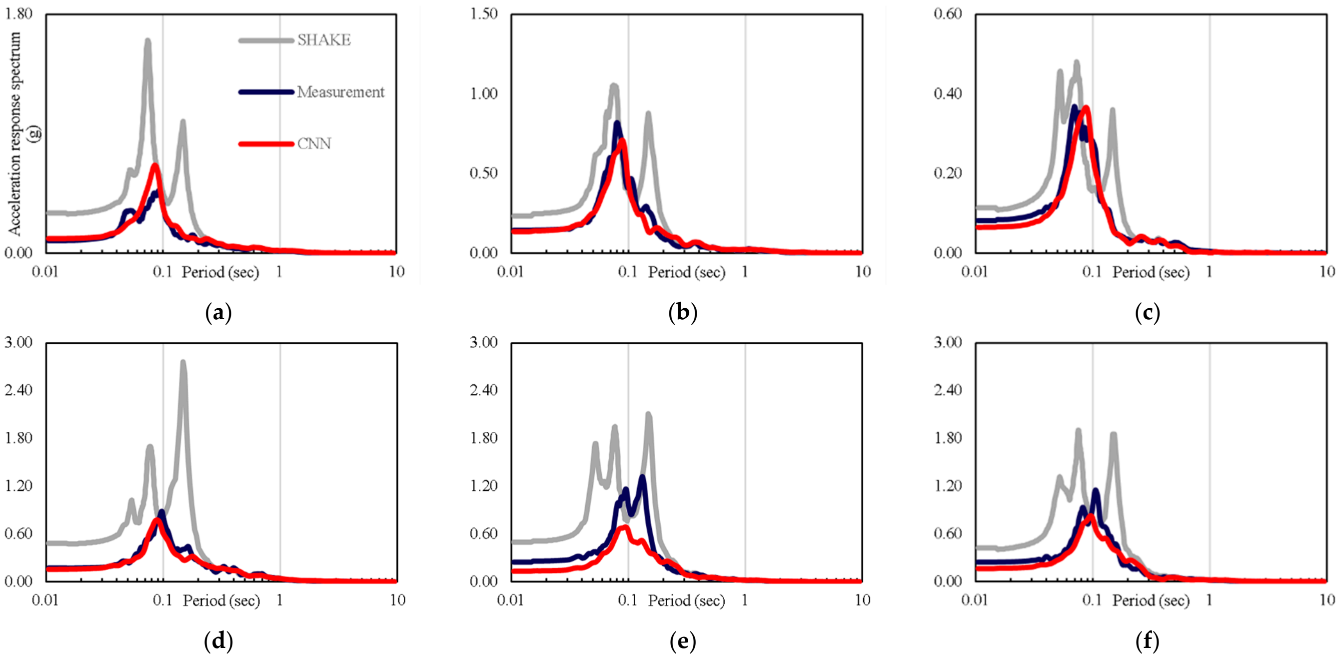

Figure 21. The six samples of acceleration response spectra measurements and predictions at site MYGH04. (**a**) MYGH041308041229.EW. (**b**) MYGH041505130613.NS. (**c**) MYGH042004200539.NS. (**d**) MYGH042102132308.EW. (**e**) MYGH042103201809.NS. (**f**) MYGH042105011027.NS.

Throughout every site, the CNN-based model predicts both values of the amplitudes and the natural periods fairly well, where the responses amplify the most with few exceptions. The proposed CNN model overestimates the response in some cases, such as (f) in Figure 10 (FKSH17), (d) in Figure 11 (FKSH18), (e) in Figure 14 (IWTH02), and (a) in Figure 17 (IWTH14), whereas it undervalued the response for (b) in Figure 11 (FKSH18), (e) in Figures 13, 20 and 21, and (f) in Figure 14 (IWTH02). On the other hand, the physical analysis software overrated most of the motions throughout the sites, especially for the site in Figure 10 (FKSH17), Figure 15 (IWTH05), Figure 18 (IWTH21), and Figure 19 (IWTH22).

5.2. Prediction Errors

An average of 20 errors in each station was calculated with Equation (7). The average errors of the estimation of CNN model and SHAKE2000 for the twelve sites are plotted in Figure 22.

$$Average\ Error = \frac{1}{n}\sqrt{\sum_{i=1}^{n}(Error_i)^2} \tag{7}$$

$$Error = SA_{pre} - SA_{test} \tag{8}$$

where n is the number of ground motions in each station ($n = 20$), $Error$ is the disparity between the response spectra estimation and the baseline of each ground motion for each site, SA_{pre} is the estimation by the models, and SA_{test} is the ground motion measurement.

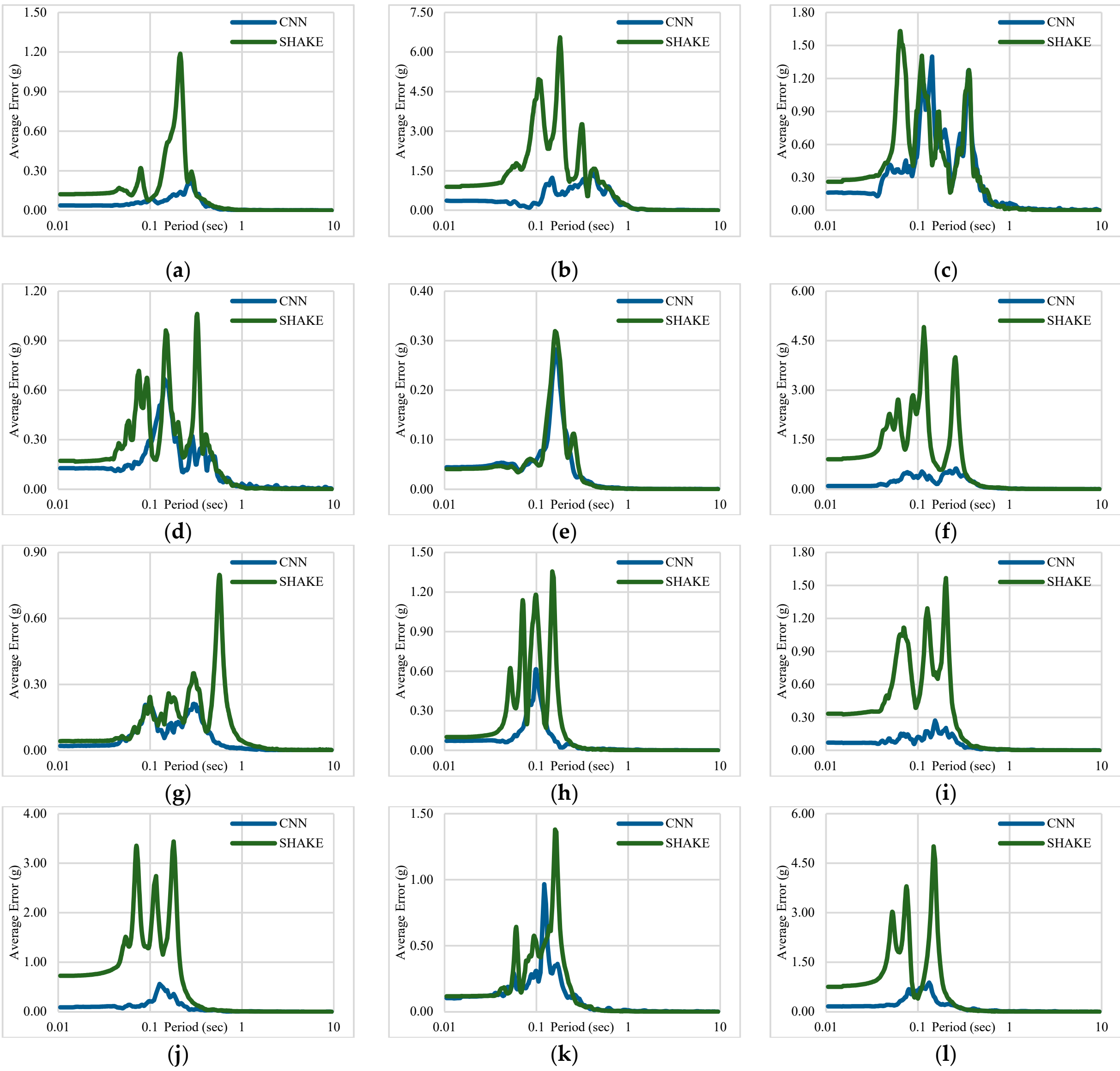

Figure 22. Average errors in the ground motions by the CNN model and SHAKE2000. (**a**) FKSH17 (**b**) FKSH18 (**c**) FKSH19 (**d**) IBRH13 (**e**) IWTH02 (**f**) IWTH05 (**g**) IWTH12 (**h**) IWTH14 (**i**) IWTH21 (**j**) IWTH22 (**k**) IWTH27 (**l**) MYGH04.

Overall, the errors of the conventional model are higher than the CNN model, especially for sites FKSH17, FKSH18, IWTH05, IWTH21, and IWTH22 in natural periods between 0.01 and 0.3 s. In addition, for sites IWTH14 and MYGH04 in natural periods between 0.01 and 0.2 s, for FKSH19 in natural periods from 0.01 to 0.1 s, for IBRH13, in natural periods from 0.3 to 0.4 s, for IWTH12, in natural periods from 0.4 to 1 s, and for IWTH27, in natural periods from 0.1 to 0.2 s. Exceptionally, it seems that there is no conspicuous gap between them throughout the whole natural periods for site IWTH02.

The global error which summarizes the total errors of the predictions for all the sites with Equation (9) are presented in Figure 23.

$$Global\ Error = \frac{1}{m}\sqrt{\sum_{j=1}^{m}\left(Average\ Error_j\right)^2} \tag{9}$$

where m is the number of sites, and $Average\ Error_j$ is an average error of 20 earthquakes in the jth station calculated with Equation (7). The proposed model especially outperforms the analysis software when the natural periods range from 0.01 to 0.3 s.

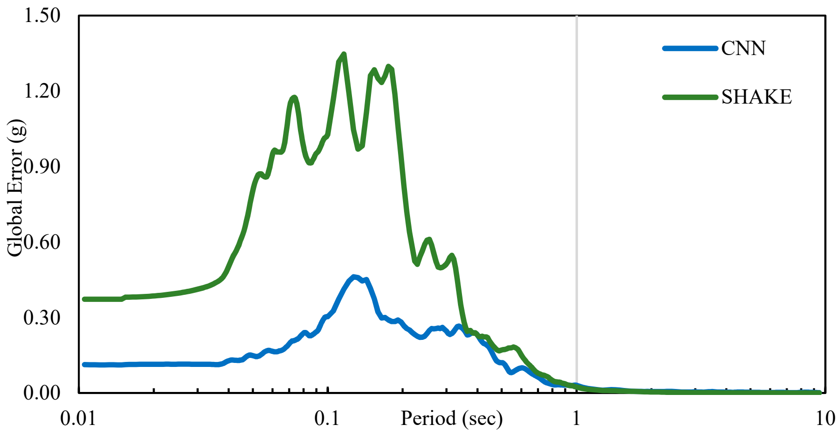

Figure 23. The global average errors of the earthquake predictions for all sites.

Moreover, the mean squared error (MSE) is utilized to represent the errors as numbers. MSE measures the average squared difference between the actual values and the estimated values with Equation (10).

$$MSE = \frac{1}{l}\sum_{k=1}^{l} Error^2 \tag{10}$$

where $Error$ is the disparity between the response spectra estimation and the baseline of each ground motion, as shown in Equation (8), and l is the number of the response spectrum values in each earthquake. An average error of 20 MSE in each station is calculated with Equation (11).

$$Average\ MSE = \frac{1}{n}\sum_{i=1}^{n} MSE \tag{11}$$

where n is the number of ground motions in each station ($n = 20$). Table 3 shows the average mean squared error of 20 response spectra estimations in each station.

For sites IWTH05, IWTH21, IWTH22, and MYGH04, the average mean squared errors of the CNN model are dozens of times lower than the errors of the software. On the other side, for sites IBRH13 and IWTH02, the values of the errors are almost the same.

Table 3. Average mean squared error of the proposed model and SHAKE2000.

Site	CNN Model	SHAKE 2000
FKSH17	0.000138	0.001734
FKSH18	0.011128	0.123401
FKSH19	0.005695	0.014009
IBRH13	0.011128	0.001150
IWTH02	0.006520	0.005750
IWTH05	0.002500	0.078644
IWTH12	0.000301	0.001670
IWTH14	0.001006	0.006529
IWTH21	0.000243	0.009845
IWTH22	0.000544	0.049496
IWTH27	0.001015	0.002871
MYGH04	0.002990	0.066302

6. Conclusions

The authors proposed two CNN-based models (A and B) to estimate the seismic response spectra of the surface. They found that model B, whose input data are acceleration, velocity, and displacement response spectra at the bedrock and output data are acceleration response spectra on the surface, outperforms model A for a site. In addition, model B does not require tailored earthquake data with the same number of values and duration. Therefore, model B for each site was trained for every selected site as a main model. Moreover, the performance of model B was compared with the result of SHAKE2000.

Among the 100 datasets in each site (12 sites) which are fabricated for the proposed model, 20 sets were used for the test. It predicts both values of the amplitudes and the natural periods fairly well, where the responses amplify the most, surpassing the performance of the physical model for all the sites with few exceptions. In particular, when the natural periods range from 0.01 to 0.3 s, the proposed model outperforms the conventional software. The average mean squared errors of the proposed model are dozens of times lower than the physical tool for specific sites. With the proposed CNN model, the evaluation of the ground response is available for sites that offer the earthquake measurements data.

As subsequent research, the authors aim at constituting a model to evaluate the surface ground motion in sites where the soil properties are available, by implementing the soil properties into the dataset.

Author Contributions: Conceptualization, J.A.; methodology, S.H.; formal analysis and software, S.H., J.J., H.-T.N. and J.A.; validation, S.H., J.J. and J.A.; investigation, S.H., H.-T.N., J.J. and J.A.; data curation, S.H., H.-T.N. and J.A.; writing—original draft preparation, S.H., H.-T.N. and J.A.; writing—review and editing, S.H., H.-T.N. and J.A. All authors have read and agreed to the published version of the manuscript.

Funding: This work is supported by the Korea Agency for Infrastructure Technology Advancement (KAIA) grant funded by the Ministry of Land, Infrastructure, and Transport (grant 21CTAP-C152100-03).

Institutional Review Board Statement: Not applicable.

Informed Consent Statement: Not applicable.

Data Availability Statement: Data are available in a publicly accessible repository that does not issue DOIs. Publicly available datasets were analyzed in this study. This data can be found here: https://www.kyoshin.bosai.go.jp, accessed on 28 May 2021.

Conflicts of Interest: The authors declare no conflict of interest.

References

1. Roeslin, S.; Ma, Q.; García, H.J. Damage assessment on buildings following the 19th September 2017 Puebla, Mexico Earthquake. *Front. Built Environ.* **2018**, *4*, 72. [CrossRef]
2. Kahandawa, K.; Domingo, N.; Park, K.S.; Uma, S. Earthquake damage estimation systems: Literature review. *Procedia Eng.* **2018**, *212*, 622–628. [CrossRef]
3. Kramer, S.L. *Geotechnical Earthquake Engineering*; Prentice Hall: Hoboken, NJ, USA, 1996.
4. Afshari, K.; Stewart, J.P. *Effectiveness of 1D Ground Response Analyses at Predicting Site Response at California Vertical Array Sites*; University of California: Los Angeles, CA, USA, 2015.
5. Yoo, J.; Hong, S.; Ahn, J. Seismic Ground Response Prediction Based on Multilayer Perceptron. *Appl. Sci.* **2021**, *11*, 2088. [CrossRef]
6. Kim, T.; Song, J.; Kwon, O.-S. Probabilistic evaluation of seismic responses using deep learning method. *Struct. Saf.* **2020**, *84*, 101913. [CrossRef]
7. Adeli, H.; Yeh, C. Perceptron learning in engineering design. *Comput. Aided Civil Infrastruct. Eng.* **1989**, *4*, 247–256. [CrossRef]
8. LeCun, Y.; Bengio, Y.; Hinton, G. Deep learning. *Nature* **2015**, *521*, 436–444. [CrossRef] [PubMed]
9. Perol, T.; Gharbi, M.; Denolle, M. Convolutional neural network for earthquake detection and location. *Sci. Adv.* **2018**, *4*, e1700578. [CrossRef] [PubMed]
10. Ross, Z.E.; Meier, M.A.; Hauksson, E.; Heaton, T.H. Generalized Seismic Phase Detection with Deep Learning. *Bull. Seismol. Soc. Am.* **2018**, *108*, 2894–2901. [CrossRef]
11. Mousavi, S.M.; Zhu, W.; Sheng, Y.; Beroza, G.C. CRED: A deep residual network of convolutional and recurrent units for earthquake signal detection. *Sci. Rep.* **2019**, *9*, 1–14. [CrossRef] [PubMed]
12. Wu, R.-T.; Jahanshahi, M.R. Deep convolutional neural network for structural dynamic response estimation and system identification. *J. Eng. Mech.* **2019**, *145*, 04018125. [CrossRef]
13. Harirchian, E.; Hosseini, S.E.A.; Jadhav, K.; Kumari, V.; Rasulzade, S.; Işık, E.; Wasif, M.; Lahmer, T. A review on application of soft computing techniques for the rapid visual safety evaluation and damage classification of existing buildings. *J. Build. Eng.* **2021**, *43*, 102536. [CrossRef]
14. Li, J.; He, Z.; Zhao, X. A Data-Driven Building's Seismic Response Estimation Method Using a Deep Convolutional Neural Network. *IEEE Access* **2021**, *9*, 50061–50077. [CrossRef]
15. NIED. *K-NET, KiK-net*; National Research Institute for Earth Science and Disaster Resilience: Ibaraki, Japan, 2019.
16. Asimaki, D.; Shi, J. *SeismoSoil User Manual*; v1.3; California Institute of Technology: Pasaneda, CA, USA, 2017.
17. Villalobos, M.; Romanel, C. Seismic Response of Soft Soil Deposit Using Simplified Models. In *E3S Web of Conferences: 2019*; EDP Sciences: Les Ulis, France, 2019; p. 16008.
18. Lee, S.-H.; Sun, C.-G.; Yoon, J.-K.; Kim, D.-S. Development and verification of a new site classification system and site coefficients for regions of shallow bedrock in Korea. *J. Earthq. Eng.* **2012**, *16*, 795–819. [CrossRef]
19. Alexander, N.; Chanerley, A.; Goorvadoo, N. A review of procedures used for the correction of seismic data. In Proceedings of the 8th International Conference on Civil & Structural Engineering, Eisenstadt-Vienna, Austria, 19–21 September 2001; ISBN 0-948749-75-X.
20. Shi, J. Improving Site Response Analysis for Earthquake Improving Site Response Analysis for Earthquake. Ph.D. Thesis, California Institute of Technology, Pasadena, CA, USA, 2019.
21. Yamashita, R.; Nishio, M.; Do, R.K.G.; Togashi, K. Convolutional neural networks: An overview and application in radiology. *Insights Imaging* **2018**, *9*, 611–629. [CrossRef] [PubMed]
22. Chopra, A.K. *Dynamics of Structures: Theory and Applications to Earthquake Engineering*; Pearson/Prentice Hall: Hoboken, NJ, USA, 2007.
23. Yoshida, N. *Seismic Ground Response Analysis*; Springer: Berlin/Heidelberg, Germany, 2015.
24. Ordonez, G.A. *SHAKE2000—A Computer Program for the 1-D Analysis of Geotechnical Earthquake Engineering Problems*; University of California: Berkeley, CA, USA, 2012.
25. Bajaj, K.; Anbazhagan, P. Identification of shear modulus reduction and damping curve for deep and shallow sites: Kik-Net data. *J. Earthq. Eng.* **2019**, *25*, 2668–2696. [CrossRef]
26. Schnabel, P.B. *Effects of Local Geology and Distance from Source on Earthquake Ground Motions*; University of California: Berkeley, CA, USA, 1973.
27. Seed, H.B.; Idriss, I.M.; Shannon, W.; Agbabian-Jacobsen, A. *Soil Moduli and Damping Factors for Dynamic Response Analyses*; EERC: Grand Forks, ND, USA, 1970.
28. Seed, H.B.; Wong, R.T.; Idriss, I.; Tokimatsu, K. Moduli and damping factors for dynamic analyses of cohesionless soils. *J. Geotech. Eng.* **1986**, *112*, 1016–1032. [CrossRef]